Adaptive Grids for Weather and Climate Models

C. Jablonowski

National Center for Atmospheric Research,
1850 Table Mesa Drive, Boulder, CO 80305, USA
cjablono@ucar.edu

M. Herzog[1], J. E. Penner[1], R. C. Oehmke[2], Q. F. Stout[2], B. van Leer[3]

University of Michigan, Ann Arbor, USA

ABSTRACT

An adaptive grid technique has been applied to a revised version of NCAR/NASA's next generation dynamical core for climate and weather research. This hydrostatic so-called Lin-Rood dynamics package is based on a conservative and monotonic finite volume discretization in flux form. The adaptive model design utilizes a spherical adaptive-grid library which is based on a cache-efficient block-structured data layout. The dynamical core is run in two configurations: the full 3D hydrostatic dynamical core on the sphere and the corresponding 2D shallow water model. This shallow water setup serves as an ideal testbed for the horizontal discretization and the 2D adaptive-mesh strategy. The static and dynamic adaptations are tested using a standard shallow water test suite and two idealized 3D baroclinic wave test cases.

1 Introduction

Adaptive Mesh Refinement (AMR) techniques provide an attractive framework for atmospheric flows since they allow improved spatial resolutions in limited regions without requiring a fine grid resolution throughout the entire model domain. The model regions at high resolution are kept at a minimum and can be individually tailored towards the atmospheric conditions.

The advantages of using nonuniform grids with increased resolution over areas of interest have been discussed in the context of atmospheric regional modeling for decades (see also *Fox-Rabinovitz et al.* [1997] for an overview). In particular, nested grids, stretched grids and dynamically adaptive mesh refinement methods have been discussed in the literature. Nested-grid approaches are widely used at National Weather Centers for detailed local forecasts. Here, a finer grid is permanently embedded in a coarse resolution model, which periodically updates the initial and lateral boundary conditions of the refined region. Even multiple nested movable grids are feasible as demonstrated by *Wang* [2001] with a primitive-equation model. This nested-grid configuration makes it possible to combine realistic large-scale simulations with mesoscale forecasts for selected regions. Such approaches can be either implemented in a one-way interaction, as in *Miyakoda and Rosati* [1977], or as a two-way interactive system (*Zhang et al.* [1986]). The former is the simplest nested-grid approach since the fine grid information does not affect the solution on the coarse grid. The latter includes a feedback mechanism that updates the coarse grid fields with the fine grid solution at any location where the two grids coincide.

Other variable-resolution models are based on the so-called stretched grid approach which can be implemented as either a statically or dynamically stretched mesh. Grid intervals outside a fine-resolution area of interest

---

[1]Department of Atmospheric, Oceanic and Space Sciences
[2]Department of Electrical Engineering and Computer Science
[3]Department of Aerospace Engineering

are then stretched uniformly over the globe (e.g. *Staniforth and Mitchell* [1978], *Côté et al.* [1998]). As a consequence, a single global variable-resolution grid is obtained that is, in the static case, held fixed during the model integrations. Non-uniform resolutions can also be achieved when applying a stretching coordinate transformation (like the Schmidt transformation proposed by *Schmidt* [1977]). Such a method together with a rotation of the poles has been investigated by *Courtier and Geleyn* [1988] and *Hardiker* [1997]. Dynamically stretched grids offer additional flexibility with respect to the chosen features of interest. They do not require prior knowledge about refinement regions and can therefore be viewed as a globally adaptive variant of the AMR approach. Dynamic grid deformations are based on time-dependent global coordinate transformations. As in the statically stretched case, the total number of grid points stays constant during the model run, but grid points can now be dynamically focused according to user-defined criteria. In atmospheric modeling, this continuous dynamic grid adaptation technique was first applied by *Dietachmayer and Droegemeier* [1992]. More recent examples include the adaptive advection tests by *Iselin et al.* [2002] and the 3D anelastic, non-hydrostatic dynamics package with grid deformations by *Prusa and Smolarkiewicz* [2003].

Dynamic AMR techniques have long been used in astrophysical, aeronautical and other computational fluid dynamics problems (*Berger and Oliger* [1984], *Berger and Colella* [1989]). However, in atmospheric science they were first applied in the late 80s when *Skamarock et al.* [1989] and *Skamarock and Klemp* [1993] published their adaptive grid techniques for 3D limited-area models in Cartesian coordinates. Recently, *Bacon et al.* [2000] and *Boybeyi et al.* [2001] introduced the adaptive non-hydrostatic regional weather and dispersion model OMEGA which addresses atmospheric transport and diffusion questions. This model is based on unstructured, triangulated grids with rotated Cartesian coordinates that can be dynamically and statically adapted to features of interest. Meanwhile, OMEGA has been used as a limited-area hurricane forecasting system in spherical geometry (*Gopalakrishnan et al.* [2002], *Bacon et al.* [2003]). Furthermore, several statically and dynamically adaptive 2D shallow water models have been proposed in the literature. Statically adaptive shallow water models on the sphere were developed by *Ruge et al.* [1995], *Fournier et al.* [2004] and *Barros and Garcia* [2004]. Dynamically adaptive shallow water models in the Cartesian x-y plane were designed by *Behrens* [1998] and *Hess* [1999]. The former uses adaptive grid triangulations whereas the latter is based on a block-structured data layout. Recently, the first AMR shallow water codes in spherical geometry have been introduced by *Jablonowski* [2004] and *Läuter* [2004].

The goal of AMR is not to move the grid globally, but rather to refine the grid locally in advance of any important physical process that needs additional grid resolution, and to coarsen the grid if the additional resolution is no longer needed. Such an approach is expected to not only capture the onset and evolution of small-scale phenomena but also to simulate the consequent large-scale small-scale flow interactions. These remain mostly unresolved by uniform grid simulations. An adaptive mesh refinement technique has been applied to a revised version of NCAR/NASA's next-generation dynamical core for climate and weather research. The governing equations and the algorithmic design of this finite-volume dynamics package are briefly reviewed in section 2. Section 3 introduces the fundamental ideas behind the adaptive mesh refinement strategy. It discusses the block-structured data layout and a new spherical adaptive mesh library for parallel computer architectures *Oehmke* [2004]). The adaptive dynamical core is run in two model configurations: the full 3D hydrostatic dynamical core on the sphere and the corresponding 2D shallow water configuration. This shallow water setup serves as an ideal testbed for the horizontal discretization and the 2D adaptive mesh strategy. The 2D test cases in section 4.1 are chosen from the standard test suite for the shallow water equations (*Williamson et al.* [1992]). Idealized 3D test cases for the adaptive dynamical core are discussed in section 4.2. In particular, the evolution of a growing baroclinic wave is assessed using two newly developed test cases. Section 5 provides a summary of the results and addresses future challenges.

2 The hydrostatic finite volume dynamical core

The hydrostatic so-called Lin-Rood finite-volume dynamical core is built upon the *Lin and Rood* [1996] advection algorithm, which utilizes advanced oscillation-free numerical approaches to solving the transport equa-

tion in flux form. In particular, *Lin and Rood* [1996] extended a Godunov-type methodology to multiple dimensions by combining a first-order upwind-biased scheme in advective form with either a second-order van Leer-type (*van Leer* [1974], *van Leer* [1977]) scheme or the third-order piecewise parabolic (PPM) method (*Colella and Woodward* [1984]) in flux form. In 1997, the conservative advection scheme became the fundamental building block of a 2D shallow water code (*Lin and Rood* [1997]) which then led to the development of the current 3D, primitive-equation based, finite-volume dynamics package.

2.1 Governing equations

The 3D dynamical core is based on a 2D shallow water approach in the horizontal plane combined with a floating Lagrangian coordinate in the vertical direction (see also discussion in *Lin* [2004]). The underlying hyperbolic shallow water system is comprised of the mass continuity equation and momentum equation as shown in equations 1 and 2. Here the flux-form of the mass conservation law and the vector-invariant form of the momentum equation are selected (see also *Lin and Rood* [1997])

$$\frac{\partial}{\partial t}h + \nabla \cdot (h\mathbf{v}) = 0 \tag{1}$$

$$\frac{\partial}{\partial t}\mathbf{v} + \Omega_a \hat{\mathbf{k}} \times \mathbf{v} + \nabla\left(\Phi + \mathcal{K} - \nu D\right) = 0 \tag{2}$$

where $\mathbf{v}$ is the horizontal (on the sphere) vector velocity with components u and v in the longitudinal (λ) and latitudinal (θ) direction and $\Omega_a = \zeta + f$ denotes the absolute vorticity. The absolute vorticity is composed of the relative vorticity $\zeta = \hat{\mathbf{k}} \cdot (\nabla \times \mathbf{v})$ and the Coriolis force $f = 2\Omega \sin\theta$ with the physical constant Ω = angular velocity of the earth. Furthermore, $\hat{\mathbf{k}}$ is the outward radial unit vector, ∇ represents the horizontal gradient operator, $\Phi = \Phi_s + gh$ symbolizes the free surface geopotential with Φ_s = surface geopotential, h = depth or mass of the fluid and g = gravitational acceleration. In addition, $\mathcal{K} = \frac{\mathbf{v} \cdot \mathbf{v}}{2}$ stands for the kinetic energy, D is the horizontal divergence and ν the divergence damping coefficient. A distinct advantage of this vector-invariant formulation is that the metric terms, which are singular at the poles in the chosen curvilinear spherical coordinate system, are hidden by the definition of the relative vorticity.

In three dimensions, the set of equations is very closely related to the shallow water system when replacing the height of the shallow water system with the hydrostatic pressure difference δp of a Lagrangian layer. Furthermore, the thermodynamic equation 4 in conservation form is added to the set

$$\frac{\partial}{\partial t}\delta p + \nabla \cdot (\delta p \mathbf{v}) = 0 \tag{3}$$

$$\frac{\partial}{\partial t}(\Theta \delta p) + \nabla \cdot (\Theta \delta p \mathbf{v}) = 0 \tag{4}$$

$$\frac{\partial}{\partial t}\mathbf{v} + \Omega_a \hat{\mathbf{k}} \times \mathbf{v} + \frac{1}{\rho}\nabla p + \nabla\left(\Phi + \mathcal{K} - \nu D\right) = 0 \tag{5}$$

where $\delta p = -\rho g \delta z$ is bounded by two Lagrangian surfaces in the hydrostatic system with density ρ and height z. The thermodynamic variable Θ is the potential temperature. The calculation of the pressure gradient forces $\frac{1}{\rho}\nabla p + \nabla\Phi$ is based on an integration over the pressure forces acting upon a finite volume. This approach constitutes the main difference between the shallow water system and the 3D model setup. The underlying method has been proposed by *Lin* [1997] and was furthermore discussed by *Janjić* [1998] and *Lin* [1998].

In this primitive-equation formulation, the prognostic variables of the dynamical core are the wind components u and v, the potential temperature Θ and the pressure thickness δp. The geopotential Φ, on the other hand, is computed diagnostically via the vertical integration of the hydrostatic relation in pressure coordinates

$$\frac{\partial \Phi}{\partial p} = \frac{-1}{\rho} \tag{6}$$

with cell-averaged density ρ. In the presence of orography as a lower boundary condition this integration then starts at the geopotential level Φ_s of the surface field. It is important to note that the hydrostatic relationship is the vertical coupling mechanism for the 2D dynamical systems in each layer. Furthermore, the pressure level p_n of each Lagrangian surface can be directly derived when adding the pressure thicknesses within the vertical column

$$p_n = p_{top} + \sum_{k=1}^{n} \delta p_k \qquad \text{for } n = 1, 2, 3, \cdots, N_{lev} \quad . \tag{7}$$

Here n denotes the vertical index starting from 1 at the lower bounding surface of the uppermost Lagrangian layer. The pressure at the model top p_{top} is prescribed and set to 2.19hPa in the current formulation. There are a total of $N_{lev} + 1$ Lagrangian surfaces that enclose N_{lev} Lagrangian layers. The concept of the floating Lagrangian surfaces is displayed in figure 1. Each layer is allowed to float vertically as dictated by the hydrostatic flow
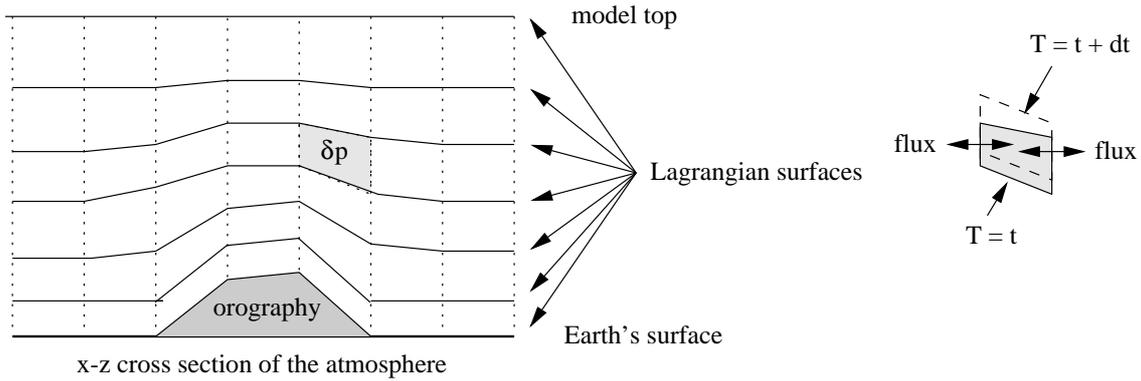
Figure 1: Terrain-following Lagrangian control-volume coordinate system of the Lin-Rood dynamical core. The pressure thickness δp of a cell is proportional to the total mass. The cell boundaries deform during the forecast (right) and after specific time intervals they are mapped back onto a fixed Eulerian reference system (not shown).

and, as a consequence, the two Lagrangian surfaces bounding the finite-volumes will deform over time. The displaced surfaces are then mapped back monotonically and conservatively to a fixed Eulerian reference system. Here, a hybrid vertical reference frame as in NCAR's Community Atmosphere Model CAM3.0 (*Collins et al.* [2004]) is chosen. The lowermost Lagrangian surface coincides with the Earth's surface field. The surface pressure is therefore automatically determined by the pressure $p_{N_{lev}}$ at the lowest level. In all 3D simulations presented in section 4.2, $N_{lev} = 26$ vertical levels have been selected.

2.2 Algorithmic design

The finite-volume dynamical core utilizes a flux form algorithm for the horizontal advection processes, which, from the physical point of view, can be considered a discrete representation of the conservation law in finite-volume space. However, from the mathematical standpoint, it can be viewed as a numerical method for solving the governing equations in integral form. This leads to a more natural and often more precise representation of the advection processes, especially in comparison to finite difference techniques. The transport processes, e.g. for the height of the shallow water system h (eqn. 1), are modeled by fluxes into and out of the finite control-volume where volume-mean quantities, as indicated by the overbar, are predicted

$$
\begin{aligned}
\bar{h}_{i,j}^{n+1} = \ & \bar{h}_{i,j}^{n} - \frac{\Delta t}{a \cos \theta_j \Delta \lambda_i} \left(F_{i+\frac{1}{2},j} - F_{i-\frac{1}{2},j} \right) \\
& - \frac{\Delta t}{a \cos \theta_j \Delta \theta_j} \left(\cos \theta_{j+\frac{1}{2}} \, G_{i,j+\frac{1}{2}} - \cos \theta_{j-\frac{1}{2}} \, G_{i,j-\frac{1}{2}} \right) \quad .
\end{aligned}
\tag{8}
$$

Here F and G denote the time-averaged 1D numerical fluxes in longitudinal and latitudinal direction which are computed with the upstream-biased and monotonic PPM scheme (see also *Carpenter et al.* [1990] and *Nair and Machenhauer* [2002]). Δt symbolizes the time step, a stands for the radius of the Earth, the indices i and j point to grid point locations in the longitudinal and latitudinal direction and the index n marks the discrete time level. In addition, $\Delta\lambda_i = (\lambda_{i+\frac{1}{2}} - \lambda_{i-\frac{1}{2}})$ and $\Delta\theta_i = (\theta_{j+\frac{1}{2}} - \theta_{j-\frac{1}{2}})$ represent the longitudinal and latitudinal grid distances measured in radians. The time-stepping scheme is explicit which allows CFL numbers less than $|CFL| < 1$. The underlying finite-volume principle of the Lin-Rood advection algorithm is discussed in *Lin and Rood* [1996]. The algorithmic details of the shallow water code and the 3D model are further described in *Lin and Rood* [1997] and *Lin* [2004].

The advection algorithm shown in equation 8 is the fundamental building block of the horizontal discretization. It is not only used to predict the time evolution of the mass (eqn. 3) and potential temperature field (eqn. 4), but also determines the absolute vorticity fluxes and kinetic energy in the momentum equation (eqn. 5).

3   Adaptive mesh refinements in spherical geometry

The AMR design is based on a block-structured data layout in spherical coordinates that allows cache-efficient, high performance computations with minimal changes to the transport algorithms of the finite-volume dynamical core. The concept of the block data structure is displayed in figure 2 that shows an orthographic projection of the Earth with a regular and block-structured grid point distribution. Each self-similar block comprises a
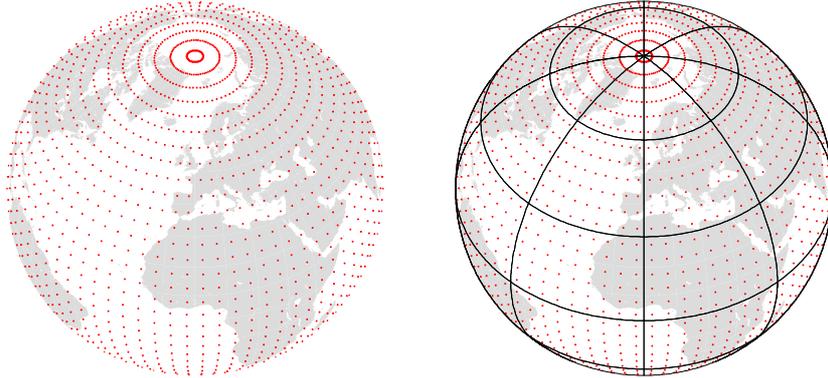
Figure 2: Distribution of grid points over the sphere (orthographic projection centered at 0E,45N), without a block-structure (left) and with the block-structure (right). The resolution is $5°$ in both figures.

constant number of $N_x \times N_y$ grid cells in longitudinal and latitudinal direction. In particular, 9×6 grid points per block are selected in the examples in section 4. The computational grid covering the Earth can then be viewed as a collection of individual blocks that are independent data units. Here the block-data principle is solely applied to the horizontal directions so that the whole vertical column is contained in a block in case of 3D model setups. Other block-data approaches, as described in *Stout et al.* [1997], *MacNeice et al.* [2000] or *PARAMESH.V3.2* [2004], employ a 3D strategy that includes a block distribution in the third dimension.

The block data structure is well-suited for adaptive mesh applications. The basic AMR principle is explained in figure 3. Starting from an initial mesh at constant resolution with for example 3×3 cells per block, a 'parent' block is divided into 4 'children' in the event of refinement requests. Each child becomes an independent new block with the same number of grid cells in each dimension, thereby doubling the resolution in the region of interest. Coarsening, on the other hand, reverses the refinement principle. Then 4 children are coalesced into a single self-similar parent block which reduces the grid resolution in each direction by a factor of 2. Both the refinement step and coarsening step are mass-conservative. In the present AMR design, neighboring blocks can only differ by one refinement level. This leads to continuously cascading refinement regions that provide a
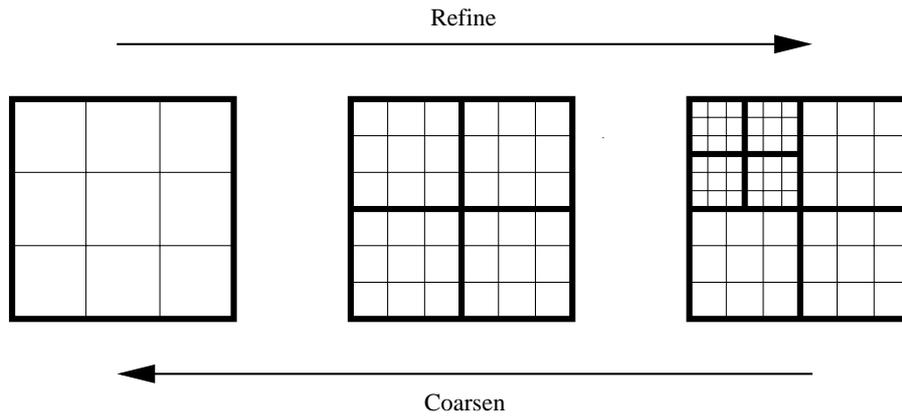
Refine

Coarsen

Figure 3: Refinement and coarsening principles with 2 refinement levels. Each block contains 3x3 cells.

buffer zone around the blocks at the finest refinement level.
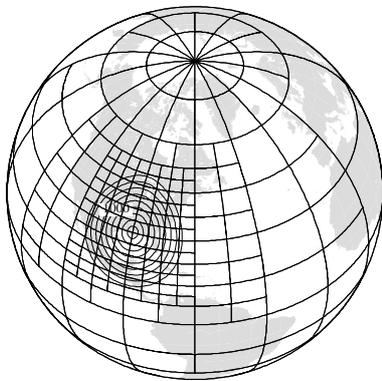
Figure 4: Adapted blocks.

An example of such a cascading grid projected onto the sphere is given in figure 4. Here a single region of interest, an idealized mountain as indicated by the contour lines, is refined at a maximum refinement level of 3. The figure clearly depicts the consequent refinement requests in order to ensure the adaptation constraint. Here, the blocks adjacent to the pole are held at a constant refinement level which enables the use of a Fourier-filtering technique in polar regions.

Each block is a logically rectangular unit with additional ghost cell regions around its boundaries. As a result, the information along adjacent block interfaces is shared which allows the use of an iterative solution procedure. The flow solver is then individually applied to all blocks within the grid before ghost cell updates along the boundaries become necessary. Here, 3 ghost cells in each direction are added in order to satisfy the requirements of the PPM solution technique. All ghost cells are at the same resolution as the parent block.

There are two types of interfaces in the adaptive grid setup as illustrated in figures 5 and 6. If the adjacent blocks are at the same refinement level (figure 5) the neighboring information can easily be exchanged since the

Ghost cells   Computational cells
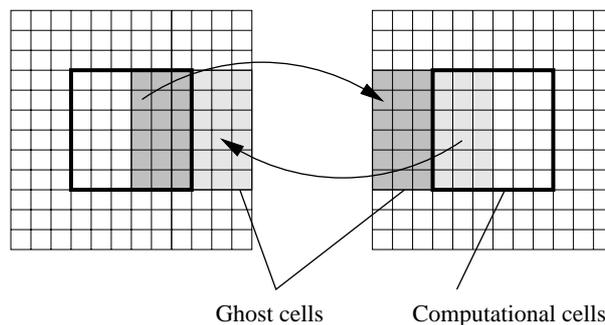
Figure 5: Ghost cell updates for blocks at the same refinement level.

data locations overlap. The ghost cell data are then assigned the appropriate solution values of the neighboring block which is indicated by the gray-shaded areas. If on the other hand the resolution changes between adjacent blocks (figure 6), interpolation and averaging routines become necessary in order to fill in the missing ghost cell information at different grid point positions. In particular, a quadratic PPM-like interpolation method is chosen which is used as a conservative and monotonic remapping technique for all cell-centered scalar variables. Special attention is also paid to the numerical fluxes across the fine-coarse grid interfaces in order to ensure
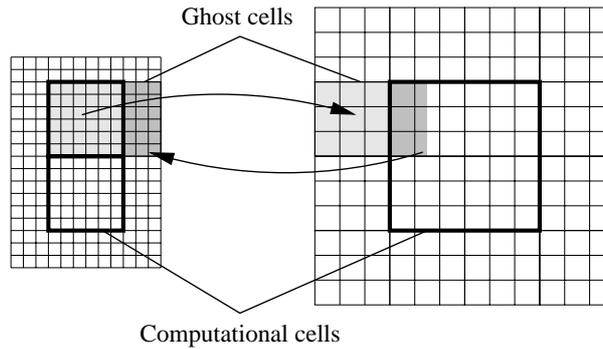
Figure 6: Ghost cell updates for blocks at different refinement levels.

conservation principles. Here a flux-matching technique is employed that averages two fine-grid fluxes and overwrites the corresponding coarse-grid flux at the boundary.

It is important to note that the adapted blocks do not overlay each other in the current setup. Instead, each block is assigned a unique surface patch on the sphere. This is in contrast to alternative AMR block-data approaches that are presented in the literature (*Berger and Colella* [1989], *Overture.v20* [2004]). For example, *Berger and Colella* [1989] reported on an AMR principle that concurrently computed the solution on all blocks at all refinement levels. The fine resolution regions then overwrote the coarse resolution data wherever the properly nested grids overlapped.

Adaptive blocks are well-suited for parallel computing concepts. Since blocks are treated as independent units they can easily be distributed among many processors. During the simulation each processor loops over its assigned blocks in order to solve the model equations on a block-by-block basis. At the end of the time step procedure the processors are synchronized which allows the update of the ghost cell regions across the communication network. All adaptive blocks are managed by a newly-developed spherical adaptive grid library for parallel computer architectures (*Oehmke and Stout* [2001] and *Oehmke* [2004]). This library defines the block-structured sphere, adapts the blocks according to user requests, loops over the blocks, maintains the adjacency information for all blocks at arbitrary refinement levels and manages the communication and load-balancing aspects on parallel computer architectures.

Self-similar blocks can be used for static and dynamic adaptations. Static refinements are placed in user-determined regions of interest, like mountain ranges or coastlines, at the beginning of a forecast. This approach even allows an accurate reinitialization of the initial data after refinements occurred, for example with an improved representation of the orography profile. Another static adaptation option is the reduced grid that statically coarsens the longitudinal resolution in polar regions. Two examples of such a grid are shown in figure 7 which illustrates the reduced grid setups with one and two reduction levels projected onto the sphere. Such a setup reduces the convergence of the meridians near the poles. Consequently, a longer time step can be used if the CFL condition near the poles limits the global time step. In addition, the overall workload of the model is reduced due to the decrease in the total number of grid points. Dynamic adaptations, on the other hand, are a powerful method when features of interest are to be tracked according to user-defined adaptation criteria. These adaptation indicators could either be based on flow characteristics or measures of the numerical truncation error. As an example, flow-dependent indicators could include assessments of the temperature, pressure or geopotential gradients as well as the vorticity and divergence of the flow field. The adaptations are then triggered if an empirical threshold is met. In sections 4.1 and 4.2, a vorticity-based dynamic adaptation criterion is tested for the 2D and 3D model setups.
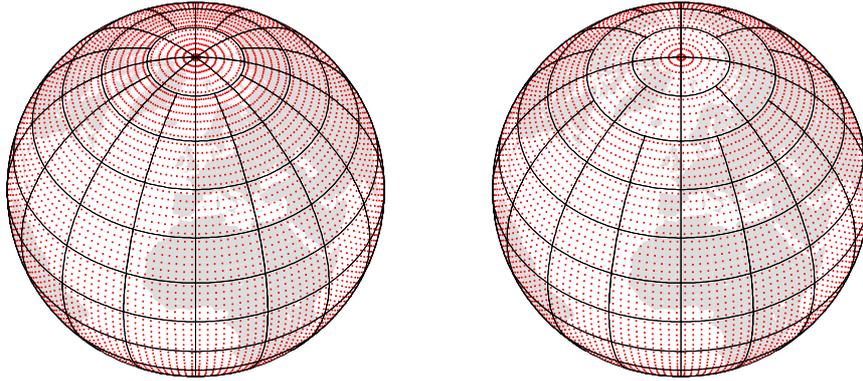
Figure 7: Distribution of blocks and grid points over the sphere (orthographic projection centered at 0E,45N). Reduced grid with 1 reduction (left) and 2 reductions (right) in the polar regions. Base resolution is $2.5° × 2.5°$.

4   Test of the AMR design

The adaptive Lin-Rood finite volume dynamical core is tested in two model configurations. First, the AMR technique is discussed in the 2D shallow water framework which reveals the main characteristics of the 2D adaptive mesh strategy. Second, the 3D hydrostatic dynamical core is assessed.

4.1   2D shallow water tests

The dynamic and static adaptations in the 2D shallow water framework are tested using the *Williamson et al.* [1992] standard shallow water test suite. Three shallow water tests with increasing complexity are selected that highlight the characteristics of the AMR design. In particular, the passive advection of a cosine bell (test case 1), a steady-state test case (test case 2) and an idealized flow over topography (test case 5) are shown. The numbers of the test cases refer to the nomenclature in *Williamson et al.* [1992]. This paper also defines the initial conditions and individual test setups.

First, the passive advection of a cosine bell with rotation angle $\alpha = 90$ is shown in figure 8 that displays the transport of the bell straight over the poles.

In this dynamically adaptive run a simple threshold adaptation criterion is applied that assesses the value of the geopotential height at each grid point. In case the geopotential height exceeds the empirical limit $h \geq 53m$ the block is flagged for refinement. This value corresponds to approximately 5% of the initial peak amplitude with $h \approx 1000m$. If on the other hand the grid points no longer meet the adaptation criterion the coarsening flag in the corresponding block is set. The refinement criterion is examined during each time step that is held variable in order to match the $|CFL| = 0.95$ limit. All adaptations occur consecutively until either the maximum refinement level or the coarse $5° × 5°$ initial resolution is reached. This resolution is the base resolution which can not be coarsened further. Here, a maximum refinement level of 3 is selected which corresponds to the grid spacing $0.625° × 0.625°$ at the finest level. It can clearly be seen that the adaptive blocks successfully capture the transport of the cosine bell as indicated by the overlaid block distribution. There are no visible distortions of the height field as the cosine bell approaches, passes over and leaves the North Pole. The increased resolution clearly helps preserve the shape and peak amplitude. A detailed discussion about the performance of the adaptive advection test with its corresponding error norms is provided in *Jablonowski et al.* [2004b]. In brief, the adapted advection tests are almost indistinguishable from the high-resolution uniform reference runs but save considerable amounts of compute time. This result has also been found by *Hubbard and Nikiforakis* [2003].

240
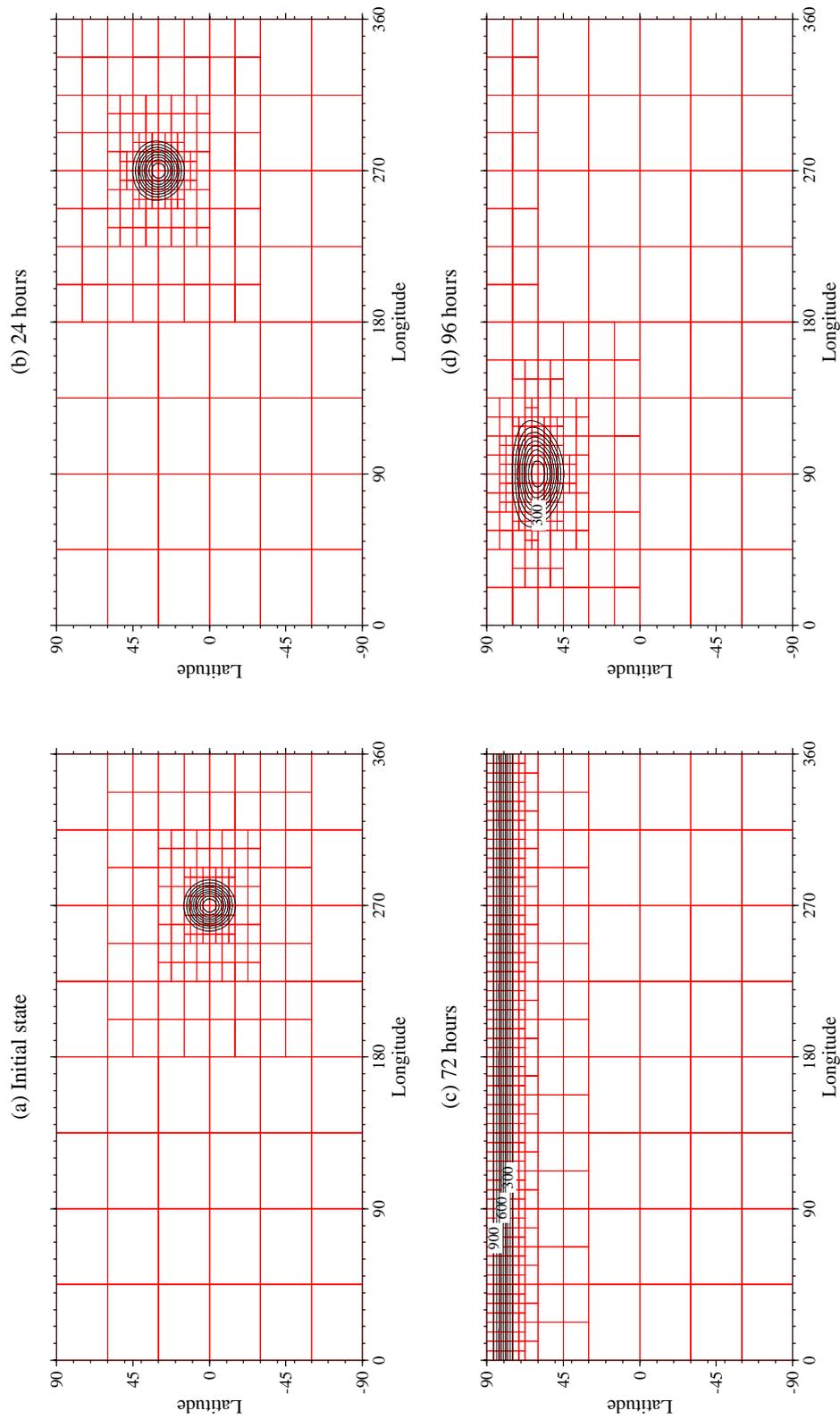
Figure 8: *Geopotential height of the cosine bell (test case 1, α = 90°) with 3 refinement levels (0.625°) at different points in time. (a) Initial state, (b) after 24 hours, (c) 72 hours and (d) 96 hours. The adapted blocks are indicated in red. Contour intervals are 100 m, the zero contour is omitted.*

Adaptive blocks can further be used for static adaptations. These are chosen in pre-determined regions of interest at the beginning of a model run and remain fixed during the simulation. They can be viewed as a two-way interactive nesting approach that provides consistent inflow and outflow conditions across the interfaces. The impact of the embedded high-resolution regions on the global domain is examined using the steady-state shallow water test case 2 with rotation angle $\alpha = 45^\circ$. Here, a high resolution refinement area at refinement level 2 is placed in the Northern Hemisphere as illustrated in figure 9. The figure shows the geopotential height
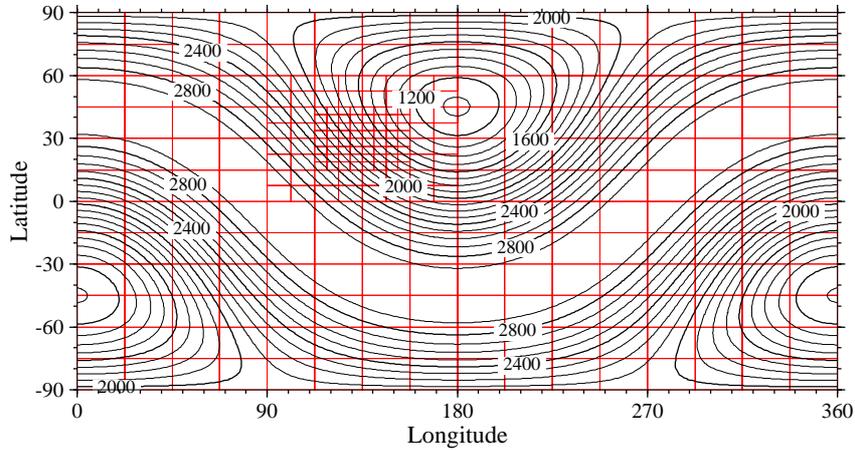
Figure 9: Geopotential height at day 14 (test case 2, $\alpha = 45^\circ$) with static refinements (refinement level 2) centered at 135E,30N. The distribution of the blocks is drawn in red. Base resolution is 2.5°, contour interval is 100 m.

field with overlaid blocks at model day 14. The base resolution in this example is a $2.5^\circ \times 2.5^\circ$ grid so that the finest resolution represents a 0.625° grid spacing. This highly idealized balanced flow pattern represents a challenge for the nested grid setup since the flow field is already well-resolved on the coarse mesh. Therefore, it is not expected that the numerical solution improves significantly in the refined region. On the contrary, the test is chosen to evaluate the model behavior at the coarse-fine grid interfaces. It can be seen that the flow passes through the refined area without noise and distortions, despite the fact that the refinements are purposely placed in a region with strong geopotential gradients. A closer examination of the wind components u and v at day 14 in figure 10 reveals that only very minor errors are induced at the coarse-fine grid interfaces. These are almost
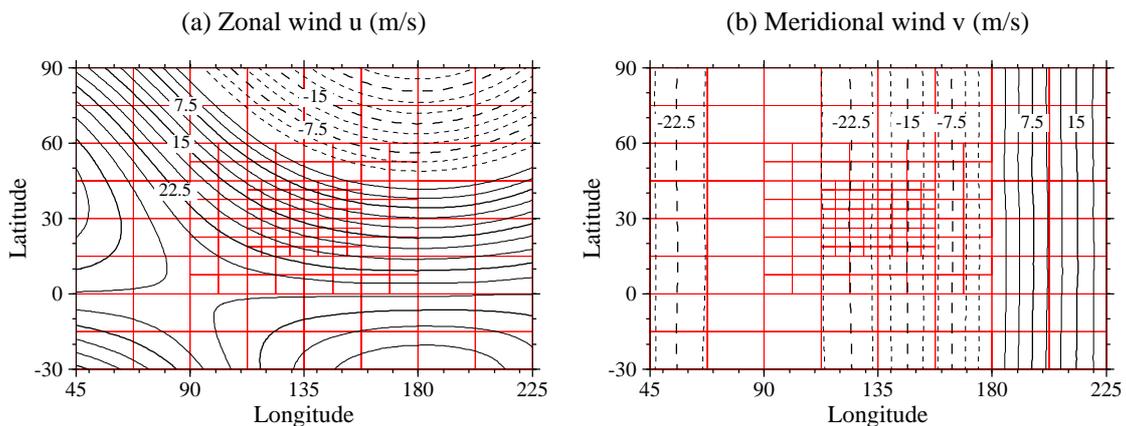
Figure 10: (a) Zonal and (b) meridional wind at day 14 (test case 2, $\alpha = 45^\circ$) with static refinements (refinement level 2). The distribution of the blocks is drawn in red. Base resolution is 2.5°, contour intervals are $2.5\,ms^{-1}$.

invisible although a slight indication of an interface effect can be detected in the v field (subfigure b). Here, the contour lines of the meridional wind show some minor fluctuations at the outflow boundary east of the refined

area. The corresponding error norms are thoroughly discussed in *Jablonowski et al.* [2004a].

The third assessment of the adaptive model design is focused on shallow water test case 5 that defines a flow over an idealized mountain. Here a dynamic refinement strategy with three refinement levels is evaluated over a forecast period of 10 days. The simulation starts with a coarse $5° \times 5°$ base resolution so that the finest mesh during the model run corresponds to a $0.625° \times 0.625°$ resolution. The adaptations are guided by a vorticity-based adaptation criterion. In particular, grid points are flagged for refinement if the absolute value of the relative vorticity exceeds the empirical threshold $|\zeta| \geq 2 \times 10^{-5} s^{-1}$. On the other hand, coarsenings are triggered if all relative vorticity values in an adapted block fall below the threshold and the neighboring blocks allow the coarsening step (compare to section 3). In case of refinements in the mountainous region the mountain height is reinitialized via analytic expression. This leads to an increase in the peak amplitude of the mountain. In general, the reinitialization of the orography profile could also be based on interpolated data. The dynamic adaptation indicator is evaluated every two model hours, which is a suitable adaptation cycle for the selected slowly evolving features of interest. In principal, an even longer time interval can also be used, for example a nine hour adaptation cycle as in *Skamarock* [1988]. These intervals allow the flow to evolve smoothly before new adaptations are applied. However, the chosen time interval must ensure that the selected feature of interest can not leave the refined region during the adaptation cycle.

Figure 11 shows three snapshots of the evolving geopotential height fields with the incorporated topography $h + h_s$ at model day 1, 5 and 10. The adapted blocks are overlaid. It can clearly be seen that the vorticity criterion picks out the lee-side wave train effectively and refines the regions with strong curvature in the geopotential height field. These regions are associated with high vorticity values. The criterion detects both troughs and ridges in the flow field since its absolute value is used for the assessments. Overall, the vorticity-based criterion is a suitable adaptation indicator for this idealized test scenario and, most importantly, the adaptive model simulation matches the NCAR high resolution reference solution (*Jakob et al.* [1993]) . An alternative refinement strategy, like the assessment of the geopotential gradient, is also a suitable choice (see discussion in *Jablonowski* [2004]).

4.2 3D dynamical core tests

The 3D hydrostatic finite volume model is assessed using two newly developed baroclinic wave test cases for dynamical cores [(*Jablonowski* [2004] and *Polvani et al.* [2004]). These deterministic test cases simulate the evolution of an isolated baroclinic wave disturbance in the Northern Hemisphere. The simulations start from a steady-state initial data set with a superimposed unbalanced perturbation. After a few days this perturbation triggers the evolution of a growing baroclinic wave with intense high and low pressure systems and strong temperature fronts. The wave ultimately breaks after approximately 9-10 model days. For these test designs, *Jablonowski and Williamson* [2004] and *Polvani et al.* [2004]) show that the solutions converge with increasing resolutions. Therefore, the model results can be compared to high-resolution reference solutions.

Figure 12 presents four snapshots of the statically adapted Jablonowski-Williamson test case. Here the surface pressure of the baroclinic wave with four different refinement levels is displayed at model day 8. The 3D evaluation of the static adaptations along the storm track in the Northern Hemisphere shows that the evolution of the baroclinic wave can be successfully predicted without noise or distortions at fine-coarse grid boundaries. The refinements capture the correct intensification of the wave train with increasing resolution without the need of a fine resolution in the global domain.

In addition to static adaptations, it is of particular interest to assess the dynamically adaptive approach without prior knowledge of the flow field. This is the classical application for adaptive mesh refinements. An example of a dynamically adapted 3D model simulation with the Polvani et al. test case is shown in figure 13. Here the maximum number of refinement levels is set to 1. The integrations cover an 8-day time period and snapshots of the surface pressure field at day 3, 4 and 8 are shown. In this example the adaptations are guided by a user-defined refinement criterion. Here a vorticity-based refinement indicator at the model level closest to the surface (at approximately 992hPa) is selected. In particular, the threshold is set to $|\zeta_{sfc}| \geq 0.75 \times 10^{-5} s^{-1}$.
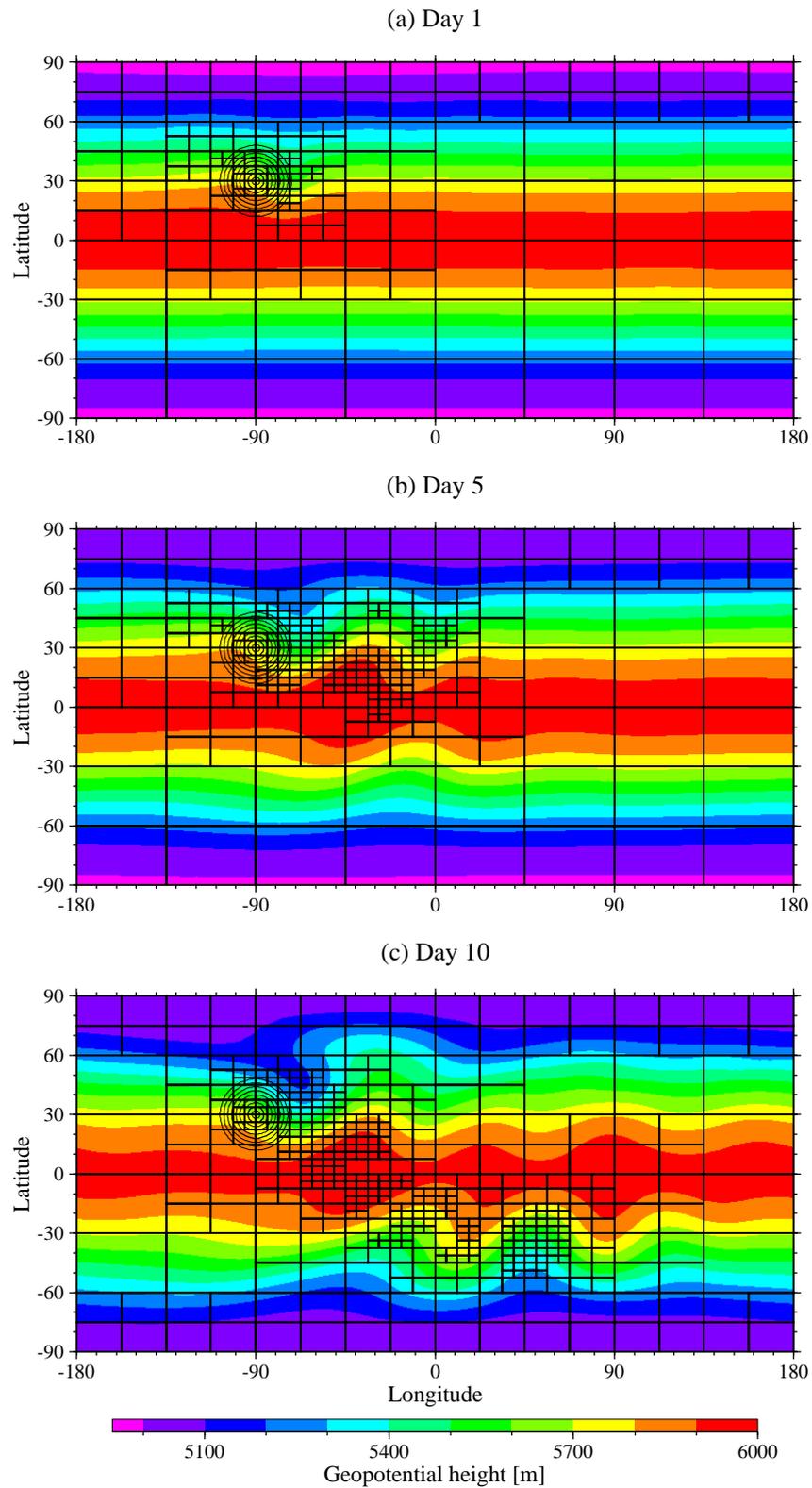
Figure 11: Geopotential height field with incorporated topography $h + h_s$ at model day (a) 1, (b) 5 and (c) 10 (test case 5). The refinement criterion is the vorticity-based indicator $|\zeta| \geq 2 \times 10^{-5}s^{-1}$. The adapted blocks are overlaid.

(a) no static refinements, finest resolution 5°x5°

(b) 1 static refinement, finest resolution 2.5°x2.5°

(c) 2 static refinements, finest resolution 1.25°x1.25°

(d) 3 static refinements, finest resolution 0.625°x0.625°
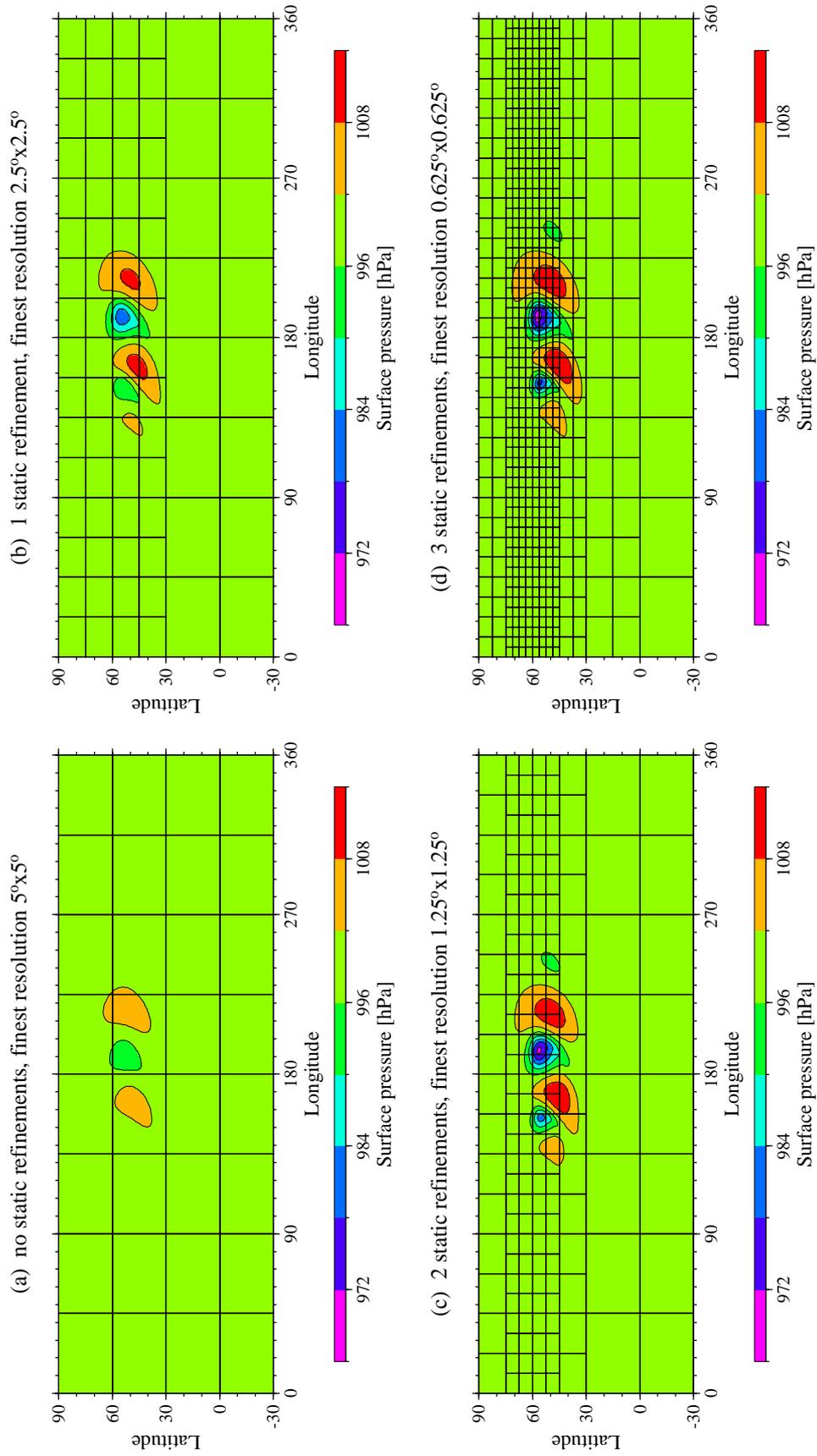
Figure 12: Surface pressure at day 8 for dynamical core runs with (a) no, (b) 1, (c) 2 and (d) 3 static refinements using the Jablonowski-Williamson test case. The adapted blocks are overlaid, the finest resolution is indicated in the titles. Contour intervals are 6hPa.
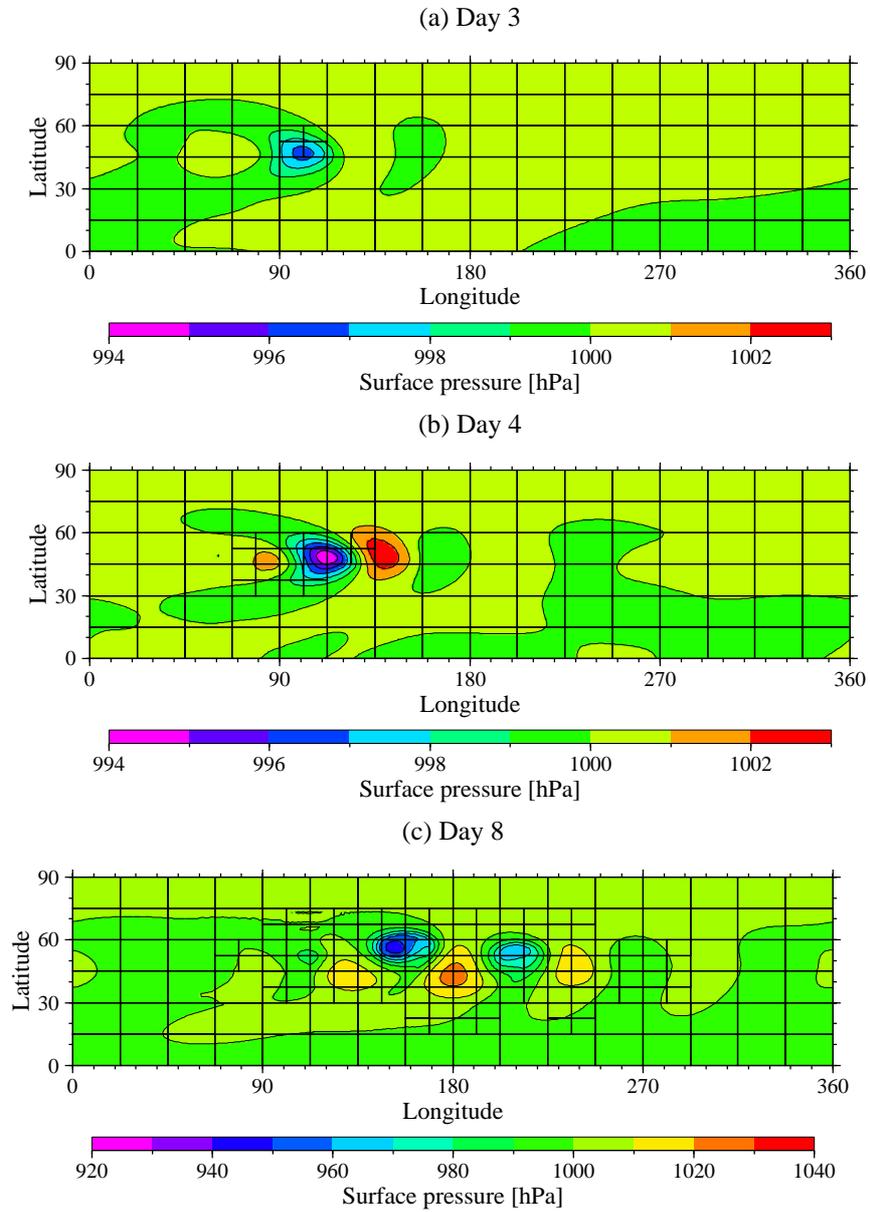
Figure 13: Surface pressure at (a) day 3, (b) day 4 and (c) day 8 for dynamical core runs with 1 dynamic refinement level using the Polvani et al. [2004] test case. The adapted blocks are overlaid, the finest resolution is $1.25° \times 1.25°$. The refinement criterion is $|\zeta_{sfc}| \geq 0.75 \times 10^{-5}s^{-1}$. Contour intervals are (a, b) 1hPa and (c) 10hPa.

This rather sensitive threshold for the absolute value of the relative vorticity is chosen in order to capture the evolution of the wave early in its developing stages. In this setup the first adaptations are triggered at model day 3. It can be seen that the refinement region clearly identifies and tracks the developing wave. As in the statically adapted case the additional resolution leads to a more accurate representation of the wave train in comparison to a uniform-grid high-resolution reference solution (not shown).

5 Conclusion and outlook

Climate and weather systems are true multi-scale phenomena that are characterized by widely varying spatial and temporal scales. Solving such a problem more efficiently and accurately requires variable resolutions that track small-scale features embedded in a large-scale flow.

A block-structured adaptive grid technique has been applied to a revised version of NCAR/NASA's finite volume dynamical core for climate and weather research. Static and dynamic adaptations have been assessed both in the 2D and 3D model framework. The 2D shallow water tests with static refinements in user-determined regions of interest have revealed that refinement regions can be successfully placed at arbitrary positions within the model domain. The flow passes through the interface boundaries without noise or significant distortions for at least a 7-14 day time period. Such a time period represents the typical duration of a weather prediction forecast. Furthermore, it was shown that dynamic refinements can successfully track a selected feature of interest. The transport of a cosine bell was well-captured and the developing wave train behind the idealized mountain in shallow water test case 5 was reliably detected by a vorticity-based adaptation criterion.

In addition, the 3D evaluations of the static adaptations along the storm track in the Northern Hemisphere have shown that the evolution of the baroclinic wave can be successfully predicted without noise or distortions at fine-coarse grid boundaries. The wave was correctly intensified due to the increase in the model resolution without the need of a fine resolution in the global domain. The dynamically adaptive baroclinic wave test confirmed that the flow is well-captured by the adapted blocks with increased accuracy in the refined region. Nevertheless, the selection of the optimal adaptation criterion and threshold is highly problem dependent and in addition, balances the computational efficiency and accuracy of the run. In general, the AMR has the potential for significant computational savings in comparison to fine-grid uniform resolution runs despite some additional workload for the AMR design.

Dynamically adaptive general circulation models on the sphere are not standard in the atmospheric science community. They are a current research trend that is pursued by research groups at the National Center for Atmospheric Research (NCAR, Boulder, Colorado, USA), the University of Cambridge (Great Britain), the Center for Atmospheric Science (Science Applications International Corporation, Virginia, USA) and the University of Michigan (Ann Arbor, MI, USA). In the future AMR climate and weather codes might offer an interesting alternative to today's uniform and nested grid approaches. If adaptive grids are capable of actually resolving selected features of interest as they appear, such as convection in tropical regions, then the corresponding parameterizations can locally be dropped and replaced by the underlying physics principles. This poses new and interesting questions concerning the small-scale large-scale flow interactions as well as possible hydrostatic and non-hydrostatic model interplays. A non-hydrostatic finite volume model is currently under development at the University of Michigan.

In the future the adaptive finite volume dynamical core will be coupled to NCAR's CAM3.0 physics package in order to assess the physics-dynamics interactions in an adaptive grid application. Here new questions about the validity of the physics parameterizations over varying grid scales will arise.

Acknowlegments

References

Bacon, D. P., et al., A dynamically adapting weather and dispersion model: The Operational Multiscale Environment Model with Grid Adaptivity (OMEGA), *Mon. Wea. Rev.*, *128*, 2044–2076, 2000.

Bacon, D. P., et al., Dynamically adapting unstructured triangular grids: A new paradigm for geophysical fluid dynamics modeling, *Proc. of the Indian Academy of Science*, *69*, 457–471, 2003, Pre-print available at URL: `http://vortex.atgteam.com/papers/`.

Barros, S. R. M., and C. I. Garcia, A global semi-implicit semi-Lagrangian shallow-water model on locally refined grids, *Mon. Wea. Rev.*, *132*, 53–65, 2004.

Behrens, J., Atmospheric and ocean modelling with an adaptive finite element solver for the shallow-water equations, *Appl. Numer. Math.*, *26*, 217–226, 1998.

Berger, M., and J. Oliger, Adaptive mesh refinement for hyperbolic partial differential equations, *J. Comput. Phys.*, *53*, 484–512, 1984.

Berger, M. J., and P. Colella, Local adaptive mesh refinement for shock hydrodynamics, *J. Comput. Phys.*, *82*(1), 64–84, 1989.

Boybeyi, Z., N. N. Ahmad, D. P. Bacon, T. J. Dunn, M. S. Hall, P. C. S. Lee, and R. A. Sarma, Evaluation of the Operational Multiscale Environment Model with Grid Adaptivity against the European tracer experiment, *J. Appl. Meteor.*, *40*, 1541–1558, 2001.

Carpenter, R. L., K. K. Droegemeier, P. R. Woodward, and C. E. Hane, Application of the Piecewise Parabolic Method (PPM) to meteorological modeling, *Mon. Wea. Rev.*, *118*, 586–612, 1990.

Colella, P., and P. R. Woodward, The Piecewise Parabolic Method (PPM) for gas-dynamical simulations, *J. Comput. Phys.*, *54*, 174–201, 1984.

Collins, W. D., et al., Description of the NCAR Community Atmosphere Model (CAM3.0), NCAR Tech. Note NCAR/TN-464+STR, National Center for Atmospheric Research, Boulder, Colorado, 2004, 214 pp., available online at `http://www.ccsm.ucar.edu/models/atm-cam/docs/description/`.

Côté, J., S. Gravel, A. Méthot, A. Patoine, M. Roch, and A. Stanisforth, The operational CMC-MRB Global Environmental Multiscale (GEM) model. Part I: Design considerations and formulation, *Mon. Wea. Rev.*, *126*, 1373–1395, 1998.

Courtier, P., and J. F. Geleyn, A global numerical weather prediction model with variable resolution: Application to the shallow water equations, *Quart. J. Roy. Meteor. Soc.*, *114*, 1321–1346, 1988.

Dietachmayer, G. S., and K. K. Droegemeier, Applications of continuous dynamic grid adaptation techniques to meteorological modeling. Part I: Basic formulation and accuracy, *Mon. Wea. Rev.*, *120*, 1675–1706, 1992.

Fournier, A., M. A. Taylor, and J. J. Tribbia, The spectral element atmospheric model: High-resolution parallel computation and response to regional forcing, *Mon. Wea. Rev.*, *132*, 726–748, 2004.

Fox-Rabinovitz, M. S., G. L. Stenchikov, M. J. Suarez, and L. L. Takacs, A finite-difference GCM dynamical core with a variable-resolution stretched grid, *Mon. Wea. Rev.*, *125*, 2943–2968, 1997.

Gopalakrishnan, S. G., et al., An operational multiscale hurricane forecasting system, *Mon. Wea. Rev.*, *130*, 1830–1847, 2002.

Hardiker, V., A global numerical weather prediction model with variable resolution, *Mon. Wea. Rev.*, *125*, 59–73, 1997.

Hess, R., Dynamically adaptive multigrid on parallel computers for a semi-implicit discretization of the shallow-water equations, GMD Tech. Report 9, GMD – German National Research Center for Information Technology, St. Augustin, Germany, 1999.

Hubbard, M. E., and N. Nikiforakis, A three-dimensional, adaptive, Godunov-type model for global atmospheric flows, *Mon. Wea. Rev.*, *131*, 1848–1864, 2003.

Iselin, J. P., J. M. Prusa, and W. J. Gutowski, Dynamic grid adaptation using the MPDATA scheme, *Mon. Wea. Rev.*, *130*, 1026–1039, 2002.

Jablonowski, C., Adaptive grids in weather and climate modeling, Ph.D. dissertation, University of Michigan, Ann Arbor, MI, 2004, Department of Atmospheric, Oceanic and Space Sciences, 266 pp.

Jablonowski, C., and D. L. Williamson, A baroclinic instabilitiy test case for atmospheric model dynamical cores, 2004, to be submitted to Mon. Wea. Rev.

Jablonowski, C., M. Herzog, J. E. Penner, R. C. Oehmke, Q. F. Stout, and B. van Leer, Adaptive grids for Atmospheric General Circulation Models: Test of the dynamical core, 2004a, to be submitted to Mon. Wea. Rev.

Jablonowski, C., M. Herzog, J. E. Penner, R. C. Oehmke, Q. F. Stout, B. van Leer, and K. G. Powell, Block-structured adaptive grids on the sphere: Advection experiments, 2004b, to be submitted to Mon. Wea. Rev.

Jakob, R., J. J. Hack, and D. L. Williamson, Solutions to the shallow-water test set using the spectral transform method, NCAR Tech. Note NCAR/TN-388+STR, National Center for Atmospheric Research, Boulder, Colorado, 1993, 82 pp.

Janjić, T., Comments on 'A finite volume integration method for computing pressure gradient forces in general vertical coordinates' by Shian-Jiann Lin (July B, 1997, 123, 1749–1762), *Quart. J. Roy. Meteor. Soc.*, *124*, 2527–2529, 1998.

Läuter, M., Großräumige Zirkulationsstrukturen in einem nichtlinearen adaptiven Atmosphärenmodell, Ph.D. dissertation, Universität Potsdam, Germany, 2004, Wissenschaftsdisziplin Physik der Atmophäre, 135 pp.

Lin, S.-J., A finite volume integration method for computing pressure gradient forces in general vertical coordinates, *Quart. J. Roy. Meteor. Soc.*, *123*, 1749–1762, 1997.

Lin, S.-J., Reply to comments by T. Janjić on 'A finite volume integration method for computing pressure gradient forces in general vertical coordinates' (July B, 1997, 123, 1749–1762), *Quart. J. Roy. Meteor. Soc.*, *124*, 2531–2533, 1998.

Lin, S.-J., A "vertically Lagrangian" finite-volume dynamical core for global models, *Mon. Wea. Rev.*, *132*, 2293–2307, 2004.

Lin, S.-J., and R. B. Rood, Multidimensional flux-form semi-Lagrangian transport scheme, *Mon. Wea. Rev.*, *124*, 2046–2070, 1996.

Lin, S.-J., and R. B. Rood, An explicit flux-form semi-Lagrangian shallow water model on the sphere, *Quart. J. Roy. Meteor. Soc.*, *123*, 2477–2498, 1997.

MacNeice, P., K. M. Olson, C. Mobarry, R. deFainchtein, and C. Packer, PARAMESH: A parallel adaptive mesh refinement community toolkit, *Comput. Phys. Comm.*, *126*, 330–354, 2000.

Miyakoda, K., and A. Rosati, One-way nested grid models: The interface conditions and the numerical accuracy, *Mon. Wea. Rev.*, *105*, 1092–1107, 1977.

Nair, R. D., and B. Machenhauer, The mass-conservative cell-integrated semi-Lagrangian advection scheme on the sphere, *Mon. Wea. Rev.*, *130*, 649–667, 2002.

Oehmke, R. C., High performance dynamic array structures, Ph.D. dissertation, University of Michigan, Ann Arbor, MI, 2004, Department of Electrical Engineering and Computer Science, 93 pp.

Oehmke, R. C., and Q. F. Stout, Parallel adaptive blocks on a sphere, in *Proc. 11th SIAM Conference on Parallel Processing for Scientific Computing*, 2001, CD-ROM. Also available online at `http://www.eecs.umich.edu/~qstout/pap/SIAMPP01.ps`.

Overture.v20, Overture home page, World Wide Web, 2004, Developers: D. Brown, W. Henshaw and D. Quinlan. Lawrence Livermore National Laboratory, Livermore, CA. URL: `http://www.llnl.gov/CASC/Overture`.

PARAMESH.V3.2, Parallel Adaptive Mesh Refinement home page, 2004, Developers: P. MacNeice, K. M. Olson, C. Mobarry, R. de Fainchtein and C. Packer. NASA Goddard Space Flight Center, Greenbelt, MD. URL: `http://ct.gsfc.nasa.gov/paramesh/Users_manual/amr.html`.

Polvani, L. M., R. K. Scott, and S. J. Thomas, Numerically converged solutions of the global primitive equations for testing the dynamical core of atmospheric GCMs, *Mon. Wea. Rev.*, 2004, In press.

Prusa, J. M., and P. K. Smolarkiewicz, An all-scale anelastic model for geophysical flows: Dynamic grid deformation, *J. Comput. Phys.*, *190*(2), 601–622, 2003.

Ruge, J. W., S. F. McCormick, and S. Y. K. Yee, Multilevel adaptive methods for semi-implicit solution of shallow-water equations on the sphere, *Mon. Wea. Rev.*, *123*, 2197–2205, 1995.

Schmidt, F., Variable fine mesh in a spectral global model, *Beitr. Phys. Atmos.*, *50*, 211–217, 1977.

Skamarock, W. C., Adaptive grid refinements for numerical weather prediction, Ph.D. dissertation, Stanford University, Stanford, CA, 1988, Department of Computer Science, 126 pp.

Skamarock, W. C., and J. B. Klemp, Adaptive grid refinements for two-dimensional and three-dimensional nonhydrostatic atmospheric flow, *Mon. Wea. Rev.*, *121*, 788–804, 1993.

Skamarock, W. C., J. Oliger, and R. L. Street, Adaptive grid refinements for numerical weather prediction, *J. Comput. Phys.*, *80*, 27–60, 1989.

Staniforth, A. N., and H. L. Mitchell, A variable-resolution finite-element technique for regional forecasting with the primitive equations, *Mon. Wea. Rev.*, *106*, 439–447, 1978.

Stout, Q. F., D. L. DeZeeuw, T. I. Gombosi, C. P. T. Groth, H. G. Marshall, and K. G. Powell, Adaptive blocks: A high-performance data structure, in *Proc. SC1997*, 1997, CD-ROM. Also available online at `http://www.eecs.umich.edu/~qstout/pap/SC97.ps`.

van Leer, B., Towards the ultimate conservative difference scheme. II. Monotonicity and conservation combined in a second-order scheme, *J. Comput. Phys.*, *14*, 361–370, 1974.

van Leer, B., Towards the ultimate conservative difference scheme. IV. A new approach to numerical convection, *J. Comput. Phys.*, *23*, 276–299, 1977.

Wang, Y., An explicit simulation of tropical cyclones with a triply nested movable mesh primitive equation model: TCM3. Part I: Model desciption and control experiment, *Mon. Wea. Rev.*, *129*, 1370–1394, 2001.

Williamson, D. L., J. B. Drake, J. J. Hack, R. Jakob, and P. N. Swarztrauber, A standard test set for numerical approximations to the shallow water equations in spherical geometry, *J. Comput. Phys.*, *102*, 211–224, 1992.

Zhang, D.-L., H.-R. Chang, N. L. Seaman, T. T. Warner, and J. M. Fritsch, A two-way interactive nesting procedure with variable terrain resolution, *Mon. Wea. Rev.*, *114*, 1330–1339, 1986.